Supporting information

High rate hybrid MnO_2@CNT fabric anode for Li-ion batteries: properties and lithium storage mechanism study by in situ synchrotron X-ray scattering

Moumita Rana,[a] Venkata Sai Avvaru,[a,b] Nicola Boaretto,[a,c] Víctor A. de la Peña O'Shea,[c] Rebeca Marcilla,[d] Vinodkumar Etacheri[a] and Juan J. Vilatela*[a]*

[a]IMDEA Materials, Eric Kandel 2, 28906 Getafe, Madrid, Spain

[b]Faculty of Science, Autonoma University of Madrid, C/ Francisco Tomás y Valiente, 7, Madrid 28049, Spain

[c]Photoactivated Processes Unit, IMDEA Energy Institute, Avda. Ramón de la Sagra 3, Parque Tecnológico de Móstoles, 28935 Móstoles, Madrid, Spain

[d]Electrochemical Processes Unit, IMDEA Energy Institute, Avda. Ramón de la Sagra 3, Parque Tecnológico de Móstoles, 28935 Móstoles, Madrid, Spain

* vinodkumar.etacheri@imdea.org, juanjose.vilatela@imdea.org

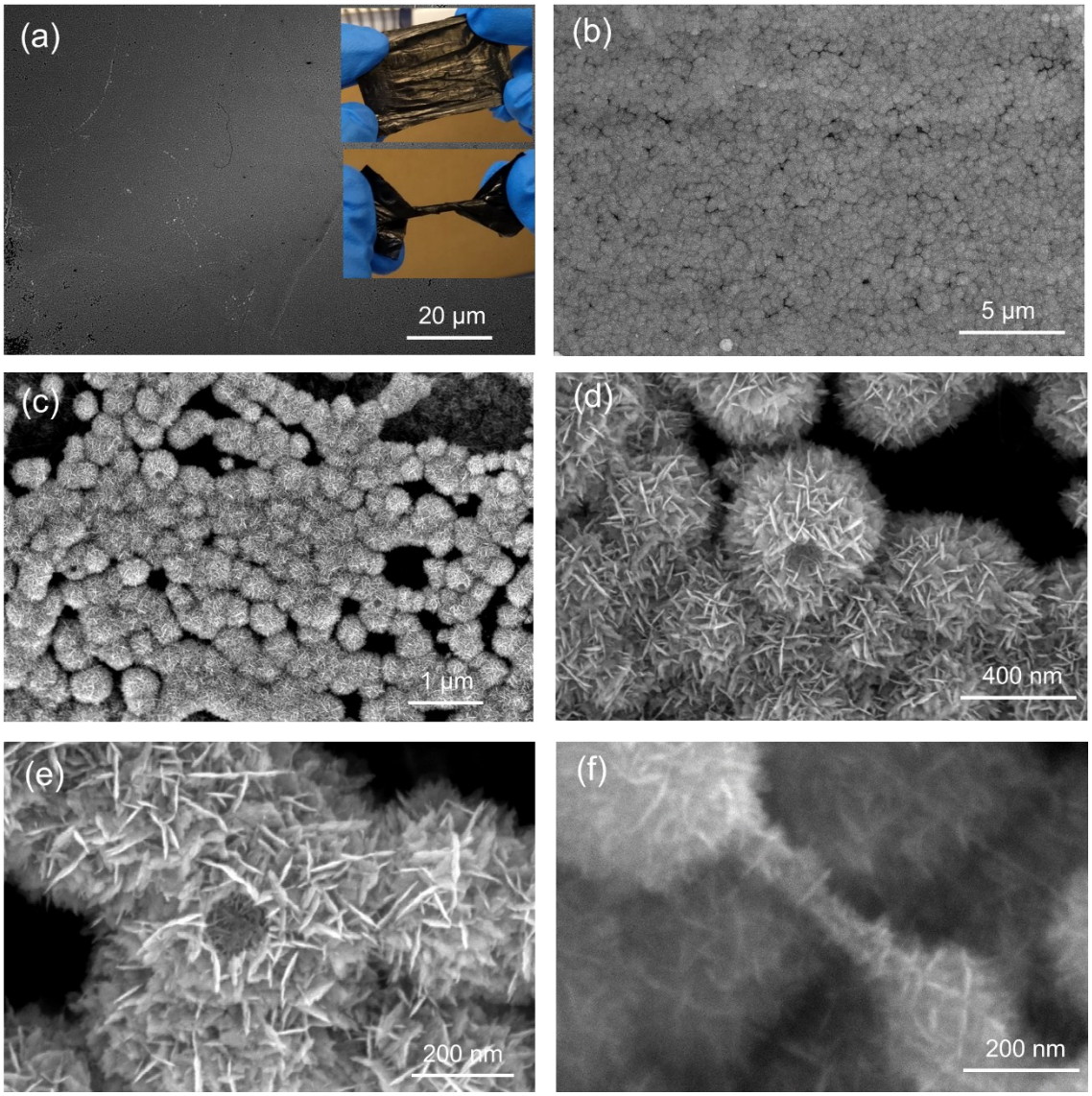

Figure S1. FESEM images of MnO_2@CNTF hybrid at different magnifications, showing inform coating of hierarchical MnO_2 nanoflowers. The preoxidized CNTF allows the uniform growth of MnO_2 as can be seen in (c) and (f). Inset pictures in (a) show the flexible nature of the macroscopic samples.

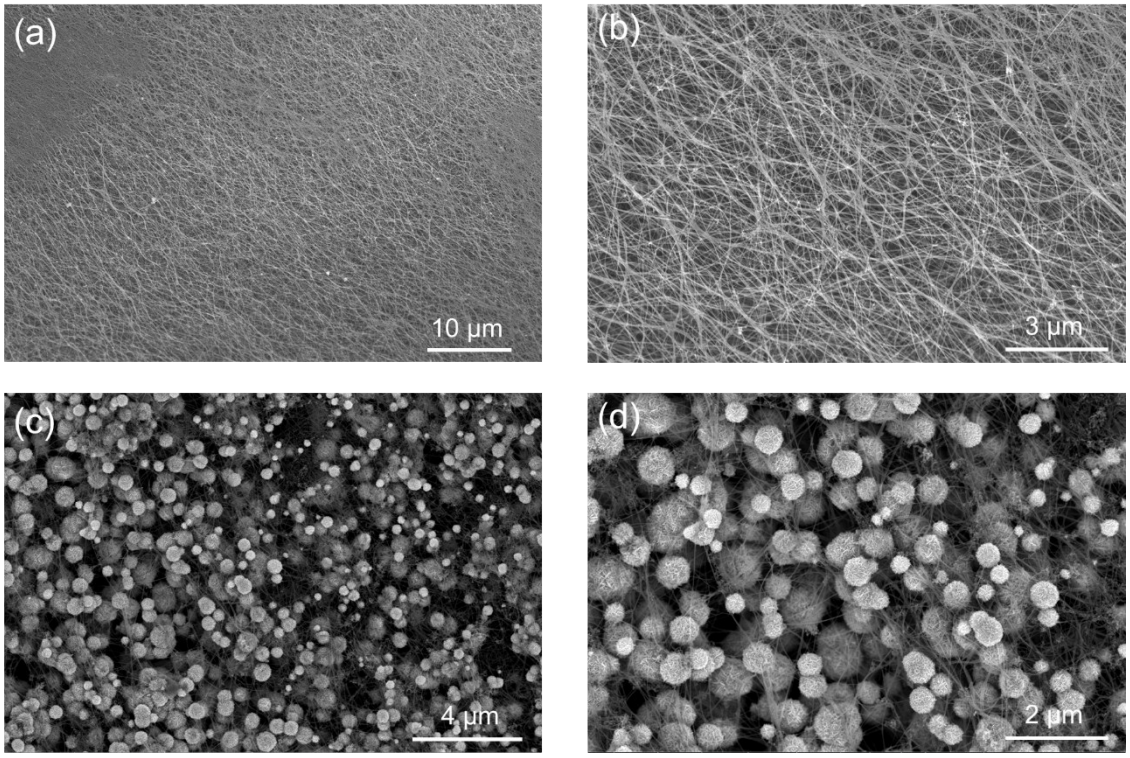

Figure S2. FESEM images of (a,b) pristine CNT fibers veils and (c,d) MnO_2 nanoflowers on pristine CNTF showing non-uniform oxide coverage on CNT bundles.

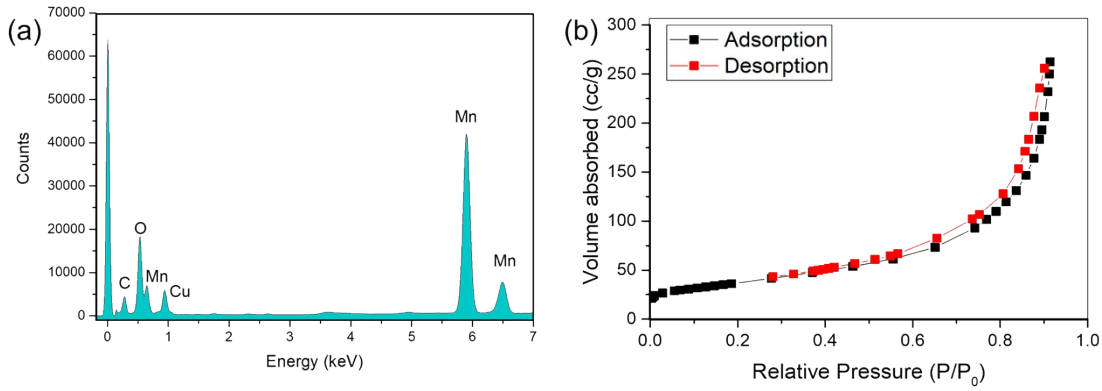

Figure S3. (a) Electron dispersive X-ray spectrum of MnO_2@CNTF hybrid. (b) BET isotherm of MnO_2@CNT hybrid.

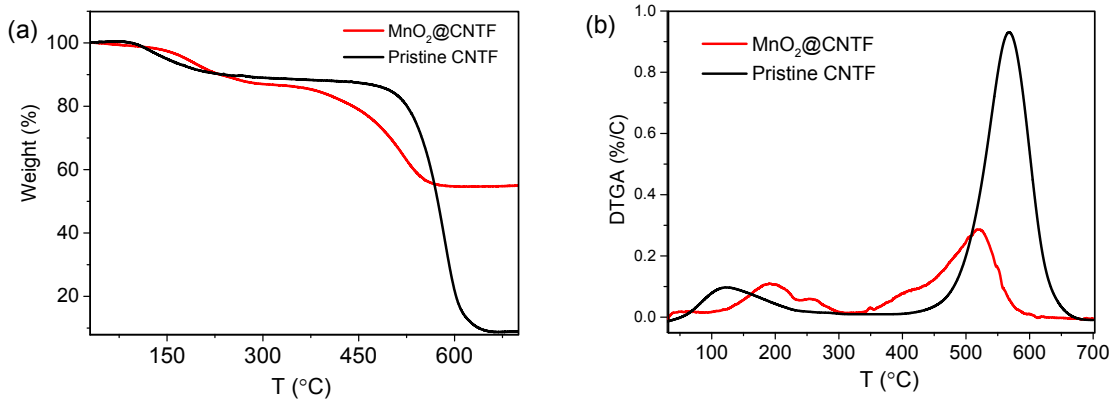

Figure S4. Comparison of (a) TGA and (b) DTA curves of MnO_2/CNTF hybrid with pristine CNTF in aerial atmosphere.

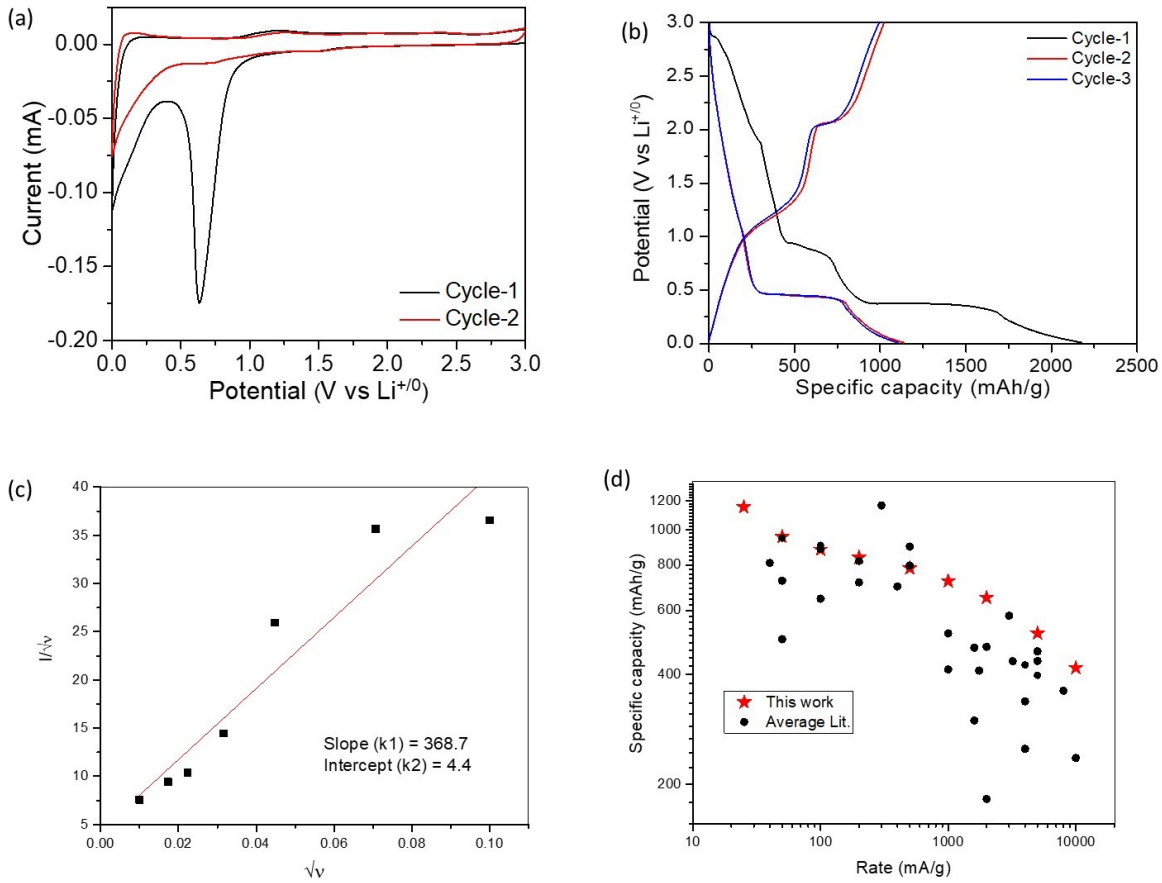

Figure S5. (a)First two cyclic voltammograms of pristine CNT at a scan rate of 0.1 mV/s. (b) First three voltage profiles of MnO_2@CNTF for charge-discharge process at a current density of 25 mA/g. (c) Fitting of Cunn-Donway (equation 1) at 2V during anodic scan (R-Square = 0.92). (d) Comparison of rating for this material and literature data (from table ST1).

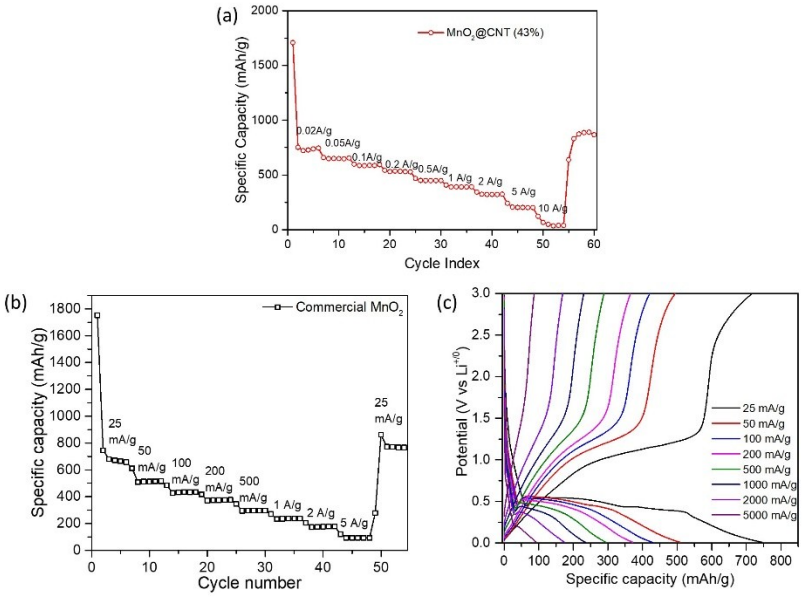

Figure S6. Rate profiles of (a) MnO_2@CNT with 43% MnO_2 loading and (b) commercial MnO_2 at current densities of 25 mA/g to 5 A/g. (c) voltage profiles of commercial MnO_2 at different current densities.

Table ST1. *Comparison of specific capacitance values of Li-ion battery anodes with MnO_2@CNTF hybrid.*

Sr. No.	***Material (crystal structure)***	***Specific capacity (mAh/g)***	***Current density***	***reference***
1.	**MnOx@CNT**	**1153**	**25mA/g**	**This work**
		955	**50 mA/g**	
		882	**100 mA/g**	
		838	**200 mA/g**	
		783	**500 mA/g**	
		722	**1 A/g**	
		650	**2 A/g**	
		519	**5 A/g**	
		344	**10 A/g**	
2.	MnO/Carbon Nanopeapods	463	5 A/g	[1]
3.	MnO_2/Carbon Nanotube Array	500	50 mA/g	[2]
4.	putty-like MnO_2/CNT	796	500 mA/ g	[3]
		236	10 A/g	
5.	MnO_2/ Conjugated Polymer/Graphene	948	50 mA/g	[4]
		698	400 mA/g	
6.	Nanoflaky MnO_2/carbon nanotube	820	200 mA/g	[5]

		250	4 A/g	
7.	Mn_3O_4/C nanospheres	1237	200 mA/g	[6]
		425	4 A/g	
8.	MnO_2 nanorods	1075	100 mA/ g	[7]
		489	1A/g	
9 .	Graphene-Wrapped MnO2–Graphene Nanoribbons	890	100 mA/ g	[8]
		550	1A/g	
10.	monodisperse α-Mn2O3 octahedra	791	100 mA/g	[9]
		435	3200 mA/g	
11.	Thin Film of Graphene-MnO2 Nanotube	495	100 mA/g	[10]
		208	1.6 A/g	
12.	Mn_3O_4–Graphene	810	40 mA/g	[11]
		390	1.6 A/g	
13.	Graphene/Ni_2P	599	100 mA/g	[12]
		260	5A/g	
14.	Mesoporous Co_3O_4	1033	100 mA/g	[13]
		622	5 A /g	
15.	MnO/C	1165	0.3 A /g	[14]
		580	3 A /g	
16.	Mesoporous Dual Carbon Armored MnO Nanoparticles	865	100 mA/g	[15]
		425	2 A/ g	
17.	Mn3O4 Nanoparticles on Hollow Carbon Nanofiber	835	200 mA/g	[16]
		528	2 A/g	
18.	(TMO = CoO, Ni_2O_3, Mn_3O4) NPs Encapsulated into B/N Co-Doped Graphitic Nanotubes	For CoO 1554	96 mA /g	[17]
		410	1.75 A /g	
19.	Hollow C sphere with open pore encapsulated MnO_2 nanosheets	780.4	500 mA/g	[18]
		398	5 A/ g	
20.	3D δ-MnO_2 nanostructure	905	0.1 A/g	[19]

		271	1 A/g	
21.	coaxial MnO_2/CNTs nanocomposite	1064	0.1 A/g	[20]
		474	1.6 A/g	
22.	Nanoflake δ-MnO_2 deposited on carbon nanotubes-graphene-Ni foam scaffolds	500	4 A/g	[21]
23.	nanostructured MnO_2	1095	100 mA/g	[22]
		464	2 A/g	
24.	MoS_2-on-MXene Heterostructures	646	100 mA/g	[23]
		182	2A/g	
		90	5 A/g	
25.	Urchin-like α-Fe_2O_3/MnO_2 hierarchical hollow composite microspheres	716	0.2 A/g	[24]
		413	1 A/g	

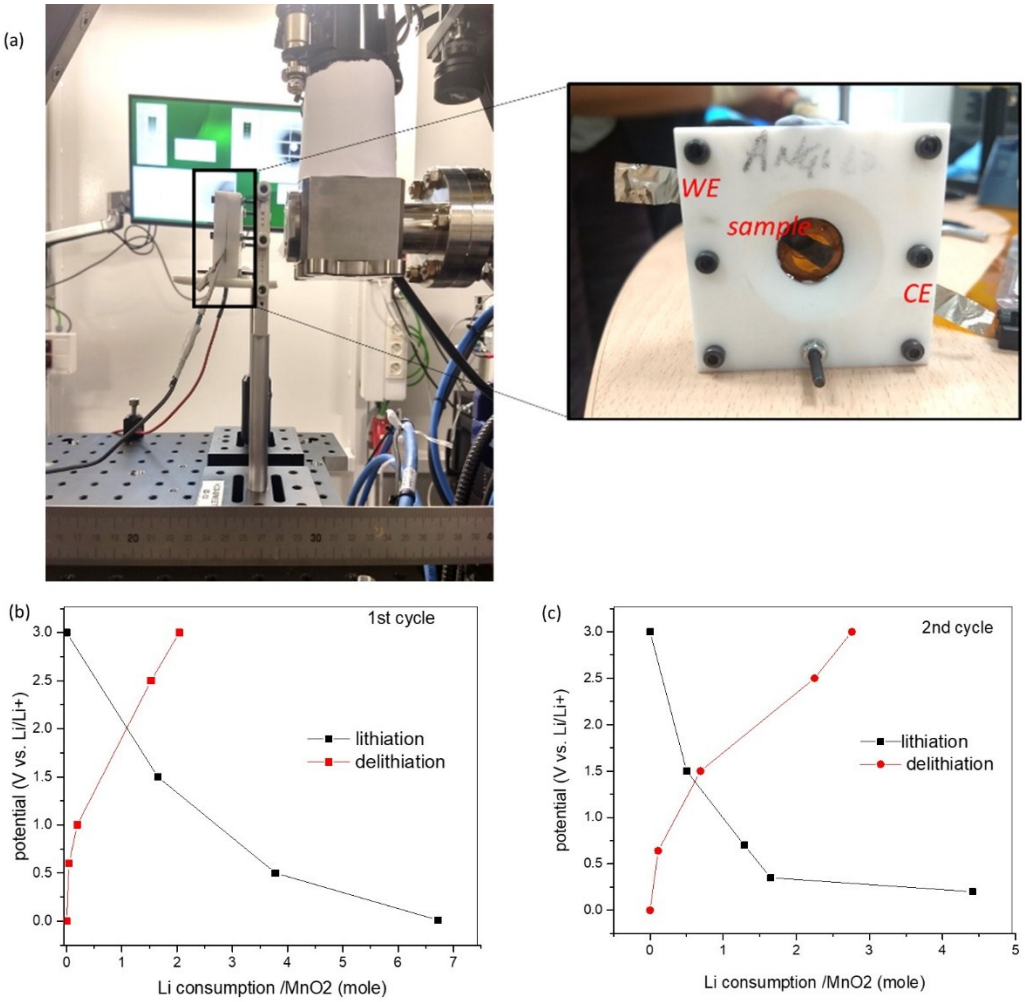

Figure S7. (a) Digital image of the set-up for the operando synchrotron SAXS/ WAXS measurements and the customized cell with free-standing working electrode. (b, c) Consumption of lithium during in situ synchrotron charge-discharge process corresponding to galvanostatic profiles shown in Figure 4.

***Table ST2**: Details of the crystallographic analysis of in situ WAXS measurement.*

Material	Crystal phase (ICSD- reference number)	Peak position in q ($Å^{-1}$)	Lattice Plane	Ref.
MnO_2	Crystal system: Hexagonal Space group: $P6_3/mmc$ a (Å): 2.829 b (Å): 2.829 c (Å): 4.410 Alpha (°): 90.0000 Beta (°): 90.0000 Gamma (°): 120 ICSD-76430, PDF 00-030-820	2.55	(100)	25
		2.92	(101)	
		3.8	(102)	
		4.42	(210)	
		5.12	(103)	
Mn_2O_3	Crystal system:Orthorhombic Space group:P b c a a (Å): 9.4120 b (Å): 9.4180 c (Å): 9.4230 Alpha (°): 90.0000 Beta (°): 90.0000 Gamma (°): 90.0000 Reference code: 98-002-4342 ICSD:24342, ICDD:00-024-0508 PDF code: 00-024-0508	2.42	(230)	26
		2.79	(114)	
		3.96	(244)	
		4.73	(435)	
		4.87	(336)	
MnO	Crystal system: Cubic Space group: F m -3 m a (Å): 4.4880 b (Å): 4.4880 c (Å): 4.4880 Alpha (°): 90.0000 Beta (°): 90.0000 Gamma (°): 90.0000 PANICSD:98-065-7312 ICSD:657312	2.45	(111)	27
		2.82	(002)	
		3.99	(113)	
		4.66	(222)	
		4.85	(004)	
$LiMnO_2$	Crystal system: Orthorhombic Space group: P m m n a (Å): 2.8050 b (Å): 4.5810 c (Å): 5.7490 Alpha (°): 90.0000 Beta (°): 90.0000 Gamma (°): 90.0000 Reference code:98-008-1050 ICSD : 81050	2.54	(012)	28
		2.95	(021)	
		4.17	(113)	
		4.91	(104)	
		5.12	(114)	

Mn	Crystal system: Cubic Space group: I -4 3 m a (Å): 8.9050 b (Å): 8.9050 c (Å): 8.9050 Alpha (°): 90.0000 Beta (°): 90.0000 Gamma (°): 90.0000 ICSD:164349, PANICSD:98-016-4349	2.62	(123)	29
		2.83	(004)	
		2.99	(114)	
		3.31	(233)	
		4.23	(244)	
		4.88	(444)	
		4.98	(055)	
$Li_{1.5}Mn_{0.97}O_2$	Crystal system: Tetragonal Space group: I 41/a m d a (Å): 5.6720 b (Å): 5.6720 c (Å): 9.1820 Alpha (°): 90.0000 Beta (°): 90.0000 Gamma (°): 90.0000 ICSD:62047, PANICSD:98-006-2047	2.33	(013)	30
		2.73	(004)	
		3.77	(132)	
		4.16	(224)	
		4.67	(026)	
Li_2O	Crystal system: Cubic Space group: F m -3 m a (Å): 4.6890 b (Å): 4.6890 c (Å): 4.6890 Alpha (°): 90.0000 Beta (°): 90.0000 Gamma (°): 90.0000 ICSD:642216, PANICSD:98-064-2216	2.32	(111)	31
		2.67	(002)	
		3.79	(022)	
		4.44	(113)	
		4.64	(222)	

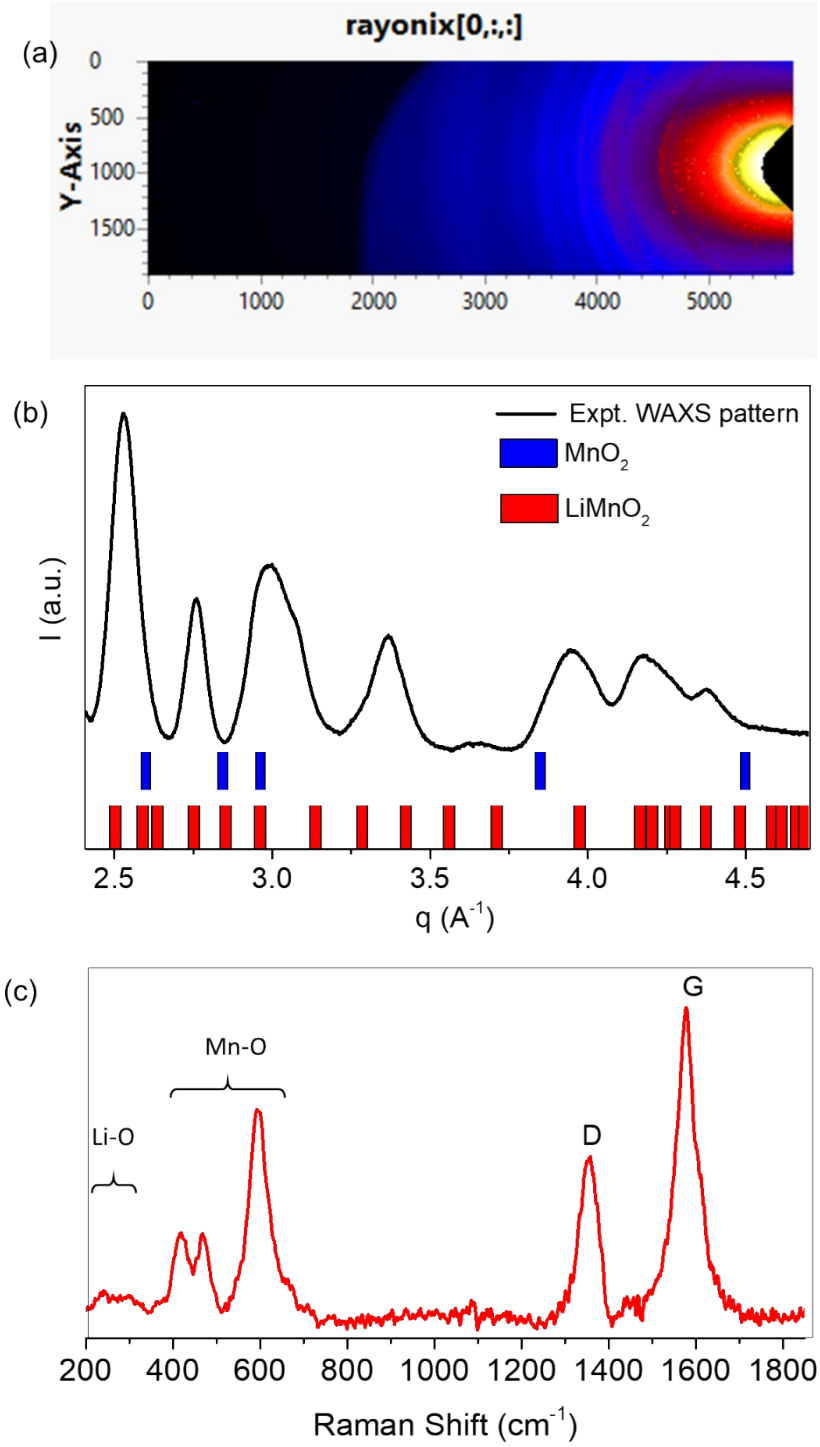

Figure S8. (a, b) WAXS pattern of electrochemically cycled MnO_2/CNTF hybrid after 60 cycles. The vertical blue and red bars indicate the simulated XRD pattern of ε-MnO_2 and $LiMnO_2$ respectively. (c) Raman spectrum of electrochemically cycled sample after 60 cycles.

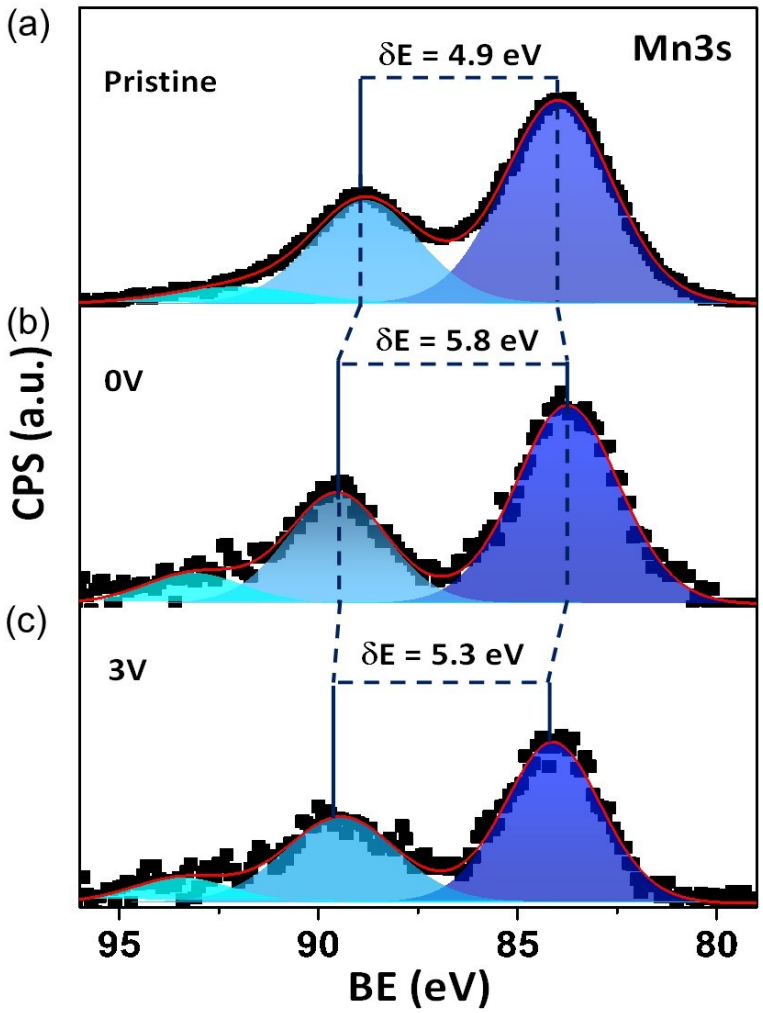

Figure S9. Convoluted XPS spectra of Mn3s recorded for (a) pristine MnO_2@CNTF, (b) sample at 0V after first lithiation and (c) sample at 3V after first delithiation.

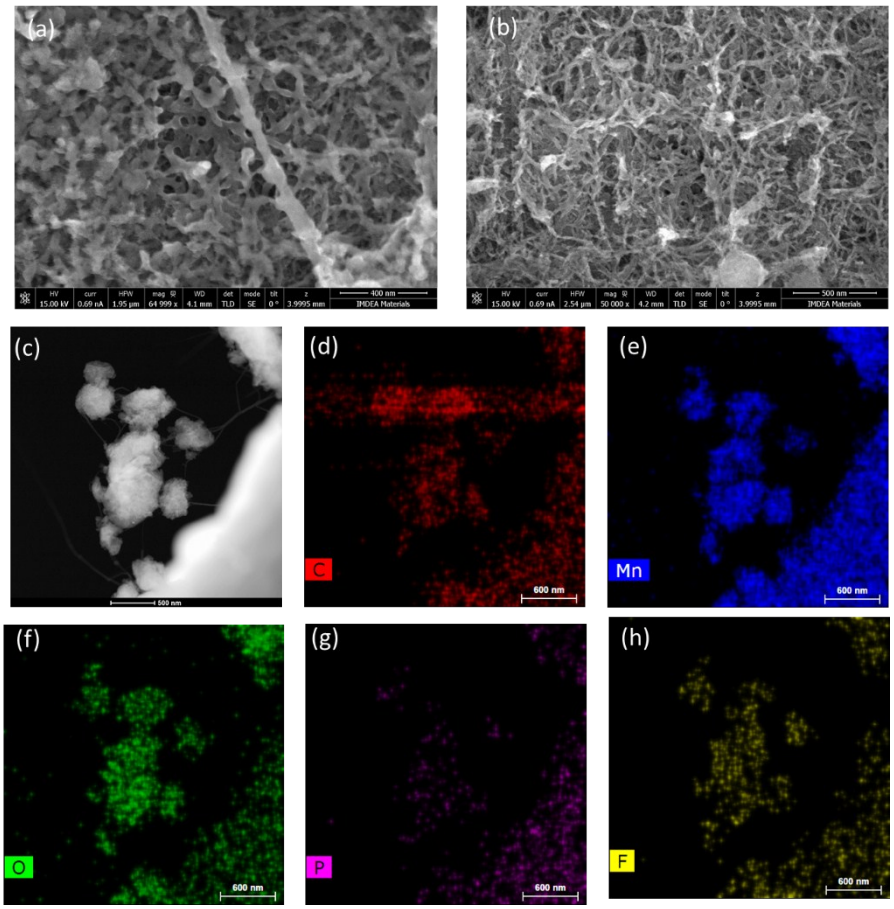

Figure S10. (a, b) FESEM images of the MnO_2@CNTF hybrid after lithiation and delithiation process. (c) HAADF and (d-h) corresponding EDS elemental mapping images for (d) carbon, (e) manganese, (f) oxygen, (g) phosphorus and (h) fluorine.

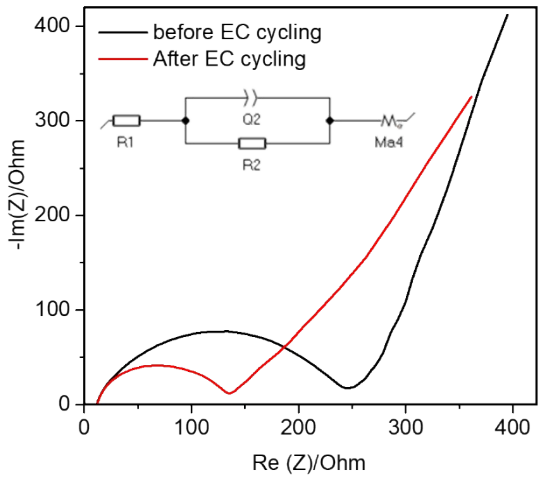

Figure S11. Comparison of the electrochemical impedance spectra (EIS) of MnO_2@CNTF before and after electrochemical cycling. Inset shows the equivalent circuit model. The fitting parameter are listed in table ST1.

Table ST3: *Fitting parameters for the EIS spectra of MnO_2@CNTF before and after potential cycling.*

Parameters	Before electrochemical cycling	After electrochemical cycling
R1 (equivalent series resistance)	11.16 Ohm	11.71 Ohm
Q2 (double layer capacitance)	13.69e-6 F.s^(a - 1)	11.76e-6 F.s^(a - 1)
R2 (charge transfer resistance)	217.7 Ohm	118.1 Ohm

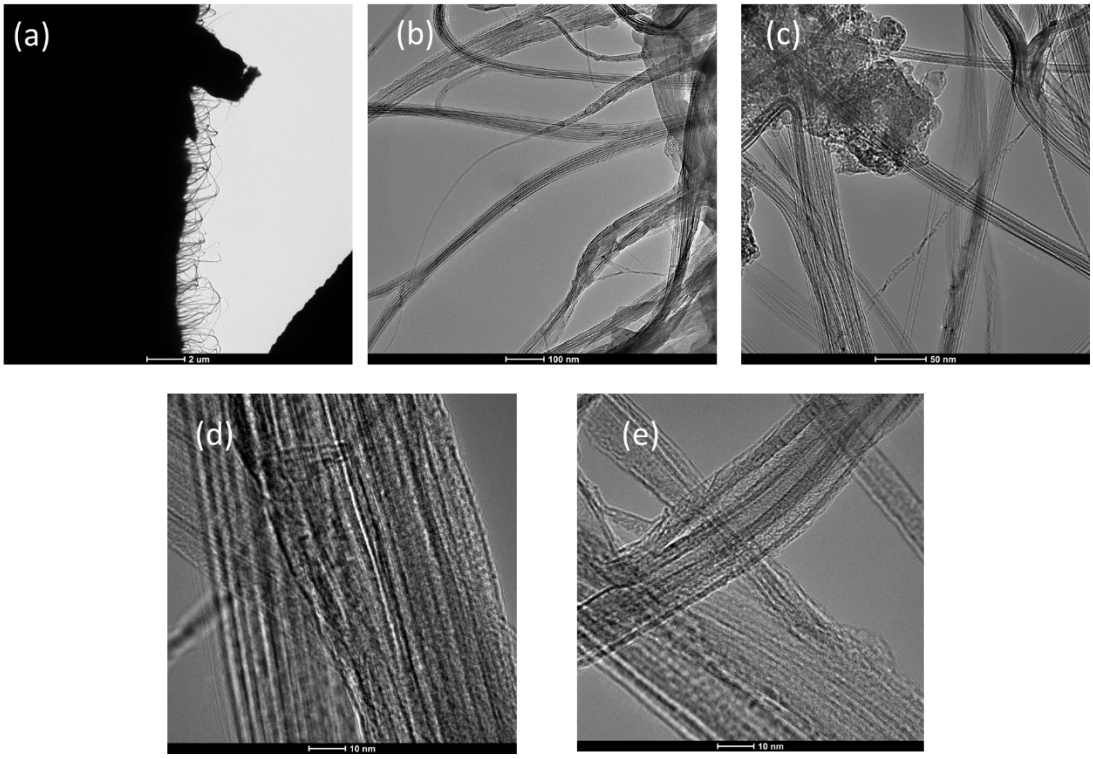

Figure S12. TEM images of the sample after CD process.

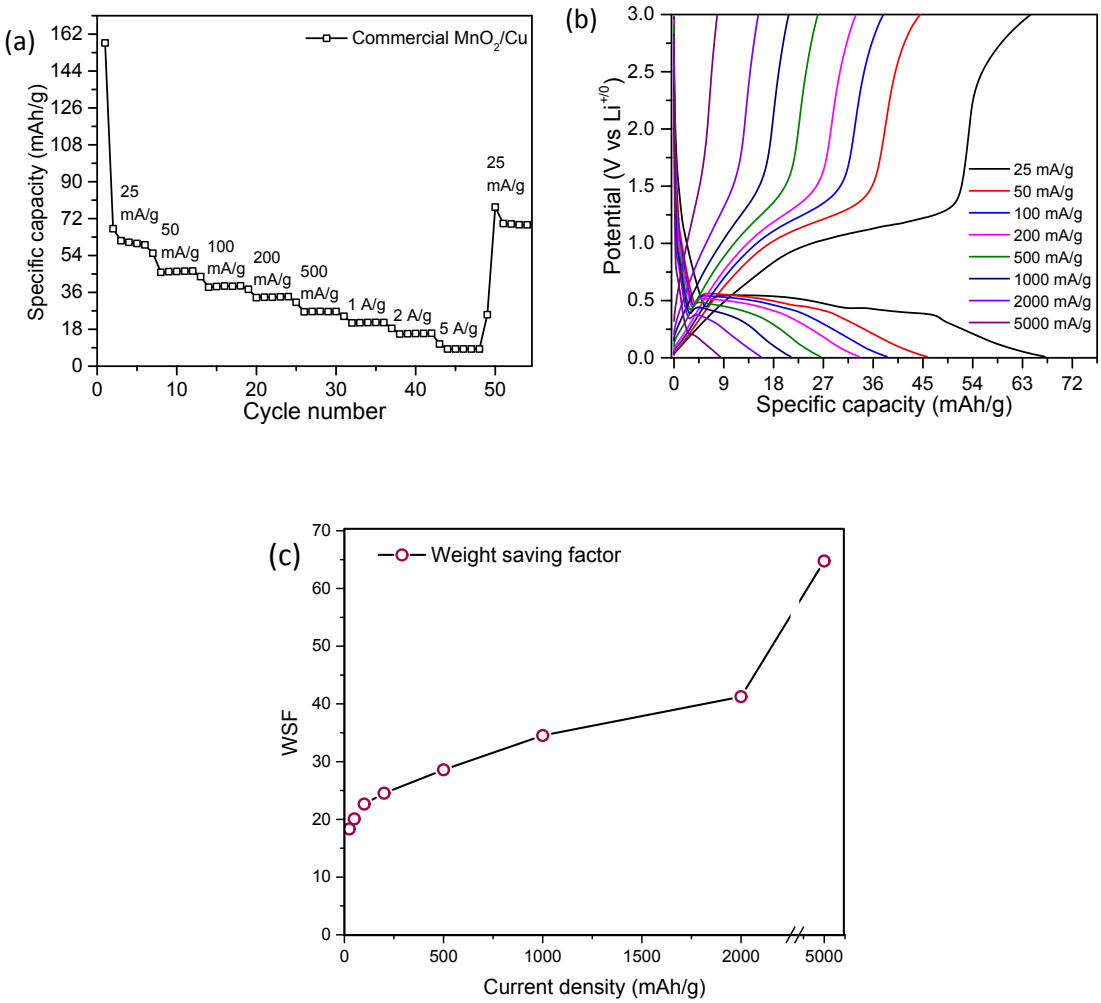

Figure S13. (a) Rate profile and (b) corresponding voltage profiles of commercial MnO2-C@Cu at different current densities. The specific capacity values are normalized with respect to the total electrode weight. (c) A plot of weight saving factor at different current densities.

References:

[1] H. Jiang, Y. Hu, S. Guo, C. Yan, P. S. Lee and C. Li, *ACS Nano*, 2014, **8**, 6038–6046.

[2] A. L. M. Reddy, M. M. Shaijumon, S. R. Gowda and P. M. Ajayan, *Nano Lett.*, 2009, **9**, 1002–1006.

[3] L. Shen, Q. Dong, G. Zhu, Z. Dai, Y. Zhang, W. Wang and X. Dong, *Adv. Mater. Interfaces*, 2018, **5**, 1800362.

[4] C. X. Guo, M. Wang, T. Chen, X. W. Lou and C. M. Li, *Adv. Energy Mater.*, 2011, **1**, 736–741.

[5] H. Xia, M. Lai and L. Lu, *J. Mater. Chem.*, 2010, **20**, 6896–6902.

[6] K. Liu, F. Zou, Y. Sun, Z. Yu, X. Liu, L. Zhou, Y. Xia, B. D. Vogt and Y. Zhu, *J. Power Sources*, 2018, **395**, 92–97.

[7] J. Chen, Y. Wang, X. He, S. Xu, M. Fang, X. Zhao and Y. Shang, *Electrochim. Acta*, 2014, **142**, 152–156.

[8] L. Li, A. O. Raji and J. M. Tour, *Adv. Mater.*, 2013, **25**, 6298–6302.

[9] J. Henzie, V. Etacheri, M. Jahan, H. Rong, C. N. Hong and V. G. Pol, *J. Mater. Chem. A*, 2017, **5**, 6079–6089.

[10] A. Yu, H. W. Park, A. Davies, D. C. Higgins, Z. Chen and X. Xiao, *J. Phys. Chem. Lett.*, 2011, **2**, 1855–1860.

[11] H. Wang, L.-F. Cui, Y. Yang, H. Sanchez Casalongue, J. T. Robinson, Y. Liang, Y. Cui and H. Dai, *J. Am. Chem. Soc.*, 2010, **132**, 13978–13980.

[12] C. Wu, P. Kopold, P. A. van Aken, J. Maier and Y. Yu, *Adv. Mater.*, 2017, **29**, 1604015.

[13] S. Zhu, J. Li, X. Deng, C. He, E. Liu, F. He, C. Shi and N. Zhao, *Adv. Funct. Mater.*, 2017, **27**, 1605017.

[14] D. Sun, Y. Tang, D. Ye, J. Yan, H. Zhou and H. Wang, *ACS Appl. Mater. Interfaces*, 2017, **9**, 5254–5262.

[15] W. Zhang, J. Li, J. Zhang, J. Sheng, T. He, M. Tian, Y. Zhao, C. Xie, L. Mai and S. Mu, *ACS Appl. Mater. Interfaces*, 2017, **9**, 12680–12686.

[16] D. Zhang, G. Li, J. Fan, B. Li and L. Li, *Chem. – A Eur. J.*, 2018, **24**, 9632–9638.

[17] H. Tabassum, R. Zou, A. Mahmood, Z. Liang, Q. Wang, H. Zhang, S. Gao, C. Qu, W. Guo and S. Guo, *Adv. Mater.*, 2018, **30**, 1705441.

[18] J. Zang, J. Ye, H. Qian, Y. Lin, X. Zhang, M. Zheng and Q. Dong, *Electrochim. Acta*, 2018, **260**, 783–788.

[19] A. A. Voskanyan, C.-K. Ho and K. Y. Chan, *J. Power Sources*, 2019, **421**, 162–168.

[20] Y. Wu, X. Li, Q. Xiao, G. Lei, Z. Li and J. Guan, *J. Electroanal. Chem.*, 2019, **834**, 161–166.

[21] X. Zhai, Z. Mao, G. Zhao, D. Rooney, N. Zhang and K. Sun, *J. Power Sources*, 2018, **402**, 373–380.

[22] L. Zhang, J. Song, Y. Liu, X. Yuan and S. Guo, *J. Power Sources*, 2018, **379**, 68–73.

[23] C. Chen, X. Xie, B. Anasori, A. Sarycheva, T. Makaryan, M. Zhao, P. Urbankowski, L. Miao, J. Jiang and Y. Gogotsi, *Angew. Chemie Int. Ed.*, 2018, **57**, 1846–1850.

[24] D. Wang, Y. Wang, Q. Li, W. Guo, F. Zhang and S. Niu, *J. Power Sources*, 2018, **393**, 186–192.

[25] Y. D. Kondrashev and A. I. Zaslavskii, *Izv. Akad. Nauk SSSR, Seriya Fiz.*, 1951, **15**, 179–186.

[26] R. Norrestam, *Wroclaw*, 2002, **1**, 1–123.

[27] M. J. Radler, J. B. Cohen, G. P. Sykora, T. Mason, D. E. Ellis and J. Faber Jr, *J. Phys. Chem. Solids*, 1992, **53**, 141–154.

[28] L. Croguennec, P. Deniard, R. Brec and A. Lecerf, *J. Mater. Chem.*, 1995, **5**, 1919–1925.

[29] A. C. Lawson, A. C. Larson, M. C. Aronson, S. Johnson, Z. Fisk, P. C. Canfield, J. D. Thompson and R. B. Von Dreele, *J. Appl. Phys.*, 1994, **76**, 7049–7051.

[30] W. I. F. David, M. M. Thackeray, P. G. Bruce and J. B. Goodenough, *Mater. Res. Bull.*, 1984, **19**, 99–106.

[31] T. W. D. Farley, W. Hayes, S. Hull, M. T. Hutchings and M. Vrtis, *J. Phys. Condens. Matter*, 1991, **3**, 4761.